Available online at www.sciencedirect.com
SCIENCE DIRECT
Polymer 45 (2004) 6495–6505
polymer
www.elsevier.com/locate/polymer

Triple-detector GPC characterization and processing behavior of long-chain-branched polyethylene prepared by solution polymerization with constrained geometry catalyst

Wen-Jun Wang[a], Semen Kharchenko[b], Kalman Migler[b,*], Shiping Zhu[a,**]

[a]*Department of Chemical Engineering, McMaster University, Hamilton, Ont., Canada L8S 4L7*
[b]*Polymers Division, National Institute of Standards and Technology, Gaithersburg, MD 20899-8544, USA*

Received 14 April 2004; received in revised form 9 June 2004; accepted 19 July 2004

Abstract

Fourteen long-chain branched (LCB) polyethylene (PE) samples were prepared by a constrained geometry catalyst. The PE samples had average branching frequencies of 0.06–0.98 branches per polymer chain, as determined by the nuclear magnetic resonance spectroscopy (^{13}C NMR). These samples, as well as five linear PEs were characterized using a gel permeation chromatography (GPC) coupled with online three-angle laser light scattering (LS), differential refractive index (DRI), and viscosity (CV) detectors. The root mean-square radius of gyration ($\langle r_g^2 \rangle^{1/2}$), intrinsic viscosity ([η]), and molecular mass (M) of the PEs were measured for each elution fraction. Based on the comparison of the long-chain branching (LCB) PEs with their linear counterparts and the Zimm–Stockmayer equation, the distributions of long-chain branch frequency (LCBF) and density (LCBD) as function of molecular mass were estimated. It was found that although the LCBF increased with the increase of molecular mass, the LCBD showed a maximum value in the medium molecular mass range for most of the PE samples. The average LCBD data from the GPC analysis were in good agreement with the ^{13}C NMR measurements. The rheological properties and processing behavior of these samples were also assessed. While the long chain branching showed significant effects on the modulus and viscosity, it did not improve the processing. Compared to linear PE, polymer melt flow instabilities such as sharkskin, stick-slip and gross melt fracture developed in extrusion of LCB PEs occurred at lower wall shear stresses and apparent shear rates.

Keywords: Polyethylene (PE); Long chain branching; Gel permeation chromatography characterization

1. Introduction

Long chain branching (LCB) is an important topic in polyolefin research. The type, length, density and distribution of branches are known to dramatically affect polymer flow behavior and processing characteristics. Understanding of the role of LCB in relation to properties of these materials is of great academic and industrial interest. Many efforts have been made to investigate branch formation in polyethylenes (PE) [1–13]. The ^{13}C NMR [1,5,14,15], rheological measurements [2–4,7], and gel permeation chromatography (GPC) (or size exclusion chromatography, SEC) coupled with on-line light scattering (LS) and/or viscosity (CV) detectors [8,9,11,12,16–22] are three major methods established to characterize long-chain branching.

The ^{13}C NMR measurement provides the estimate of the long-chain branching density (LCBD) and frequency (LCBF). The former is the ratio of the number of branch points over that of total carbons, while the latter is the number of branch points per polymer molecule. This quantitative method is limited to identifying methylene units less than six carbons adjacent to a branched methine [1,14].

Rheological properties are very sensitive to the presence of long chain branches in polymer samples, and are known to provide qualitative information about branching [2–4,7]. The zero-shear viscosity, storage (G') and loss modulus

* Corresponding authors. Tel.: +1-301-975-4876; fax: +1-301-975-4924. ** Tel.: +1-905-525-9140x24962; fax: +1-905-521-1350 (S. Zhu).
E-mail addresses: Kalman.migler@nist.gov (K. Migler), zhuship@mcmaster.ca (S. Zhu).

0032-3861/$ - see front matter © 2004 Elsevier Ltd. All rights reserved.
doi:10.1016/j.polymer.2004.07.035

(G''), as well as shear-thinning behavior vary with LCB. However, the interpretation of rheological data requires a good understanding of branch type and level.

The LCB can also be identified by a comparative measurement of polymer hydrodynamic volume in a dilute solution [8,9,11,12,16–21]. A branched chain (br) assumes more compact gyration than its linear counterpart (lin) having the same molecular mass (M). It has lower root mean-square radius of gyration ($\langle r_g^2\rangle^{1/2}$) [23] and intrinsic viscosity ($[\eta]$) [24] than a linear one. With the help of the GPC coupled with LS and viscometer, the LCB distribution can be elucidated quantitatively from the contraction factors (g, g'):

$$g = \left(\frac{\langle r_g^2\rangle_{br}}{\langle r_g^2\rangle_{lin}}\right) \quad (1)$$

$$g' = \left(\frac{[\eta]_{br}}{[\eta]_{lin}}\right) \quad (2)$$

Among various LCB PEs, the polymers produced by constrained geometry catalysts (CGC) have narrow molecular mass distributions. The average LCBD levels in the CGC PEs are typically less than one branch per polymer molecule [1,5]. Characterizing such low-level LCB PE samples provides a great challenge to polymer scientists.

In this work, we prepared a series of LCB PE samples by high-temperature solution polymerization process using a CGC system. We then characterized these samples by the GPC coupled with the three on-line detectors: three-angle laser light scattering (LS), differential reflective index (DRI) and viscometer (CV). Five linear PE samples including one NBS 1475a standard were also investigated for comparison. The major objective is to determine if LCB density is molecular mass dependent. Longer PE chains are expected to have higher LCBF (number of branches per chain), but what about LCBD (number of branches per 10,000 carbons)? Would doubling molecular mass yield twice as many branches? If not, would it be higher or lower? This information is of the fundamental value because it provides insights into the mechanisms of the branch formation during polymerization. Another objective is to evaluate the effects of long chain branching on the materials rheological properties as well as flow instabilities, such as sharkskin, stick-slip and gross melt fracture that are relevant to processing of these materials.

2. Experiment part

2.1. Sample preparation

The synthesis and molecular characterization was performed at McMaster University. Fourteen LCB PE samples were synthesized in a high-temperature, high-pressure continuous stirred-tank reactor system (CSTR) using a CGC-Ti system, i.e. $[C_5Me_4(SiMe_2N^tBu)]TiMe_2$ (Me: methyl, ^{t}Bu: t-butyl, C_5: cyclopentadiene) (CGC-Ti provided by Dow Chemical [38] as a 10% (by mass fraction) solution in Isopar E)/tris(pentafluoro phenyl)boron (TPFPB provided by Dow Chemical as a 3% (by mass fraction) solution in Isopar E)/modified methylaluminoxane (MMAO-3A with a 29% (by mass fraction) isobutyl content, provided by Akzo-Nobel as a 7.2% (by mass fraction) aluminum in heptane), and a binary catalyst system of CGC-Ti and zirconocene dichloride (Strem Chemicals). Four linear PE samples were also prepared in the CSTR with zirconocene dichloride-modified methylaluminoxane, and the NBS 1475a linear PE was purchased from the National Institute of Standards and Technology. More detailed description of the synthesis procedure can be found elsewhere [1,10,25].

2.2. ^{13}C NMR measurements

The 75.4 MHz ^{13}C NMR spectra were acquired on a Bruker AC 300 pulsed NMR spectrometer with completed proton decoupling at 120 °C. The LCBD for the CGC PE samples were in the range of (0.20–2.88) carbons per 10,000 carbons, and the LCBF were (0.06–0.98) carbons per polymer molecule [1,10]. LCBF was estimated from LCBD and M_n by $2\times\text{LCBD}\times M_n/28$, where 2 accounts for one ethylene having two carbons, and 28 is ethylene molecular mass. The linearity of four zirconocene PE samples was also confirmed by the ^{13}C NMR. Only very low levels of methyl branches (about three branches/10,000 carbons) were found in these samples.

2.3. Triple detector array GPC measurements

Seven narrow polystyrene (PS) standards (Tosoh Corp.) with molecular masses from 870 to 1.09×10^6 g/mol and M_w/M_n of about (1.01–1.11) and two PS standards from Pressure Chemical [38] with M_w of (3 and 20)$\times10^4$ g/mol and M_w/M_n less than 1.06 were also used for the purposes of the universal calibration, detector delay volume measurement, and normalization of LS data. All samples were dissolved in spectrophotometric grade 1,2,4-trichlorobenene (Aldrich) and stabilized by the 0.01% mass fraction of Irganox 1010 (Ciba). The solvent was filtered and the sample solutions were kept at 150 °C for 4 h before loading into the SEC carousel.

All experiments were conducted in a Waters Alliance GPCV 2000. In addition to a differential reflective index detector (DRI) and three capillary viscometer detectors (CV), a three-angle laser light scattering detector (TALLS, high temperature mini-DAWN from Wyatt technology) was installed on-line in the SEC. Three detection angles were 45, 90 and 135° and the laser wavelength was 690 nm. The detectors were arranged in a series: TALLS, DRI, and CV. The delay volumes between TALLS and DRI, and between DRI and CV were (0.200 and 0.074) ml, respectively. The

DRI increment dn/dc was 0.047 ml/g for PS and −0.104 for PE [11,26]. A set of four Styragel HT 6E linear columns (Waters) was used. All experiments were carried out at 135 °C. The solvent was filtered using a 0.22 μm filtration system and passed through an inline filter prior to entering the columns at a fixed flow rate of 1.0 ml/min at 135 °C. The SEC traces from three detectors for Sample CGC1 are shown in Fig. 1.

The CV detector measures the relative viscosity with its three-capillary design. The $C_i[\eta]_i$ values (C_i: polymer concentration, $[\eta]_i$: intrinsic viscosity) in each elution fraction as a function of the elution volume was thus obtained directly. Coupled with the concentration information at the same elution volume from the DRI detector, the relationship between $[\eta]$ and elution volume was determined.

2.4. Radius of gyration

The LS detector measures the excess Rayleigh ratio (R_θ). The Zimm method was used to evaluate the molecular mass M_i and the root-mean-square radius of gyration $[(\langle r_g^2\rangle)^{1/2}]_i$ for each elution fraction [27]. The expression for the angular θ dependence of R_θ in a dilute polymer solution can be written as (note: the second virial term is negligible in this study due to extremely low C),

$$\frac{K^*C}{R_\theta} = \frac{1}{MP(\theta)} \tag{3}$$

where K^* is an optical constant and can be expressed as $4\pi^2 n_0^2 (\mathrm{d}n/\mathrm{d}c)^2 \lambda_0^{-4} N_A^{-1}$, n_0 is the solvent refractive index at the incident radiation (vacuum) wavelength of λ_0, N_A is the Avogadro's constant, and $P(\theta)$ is the theoretically derived form factor that equals to $1 - \left[4\pi\lambda_0^{-1}\sin(\theta/2)\right]^2\langle r_g^2\rangle/3 + \cdots$. The plot of K^*C/R_θ versus $\sin^2(\theta/2)$ gives

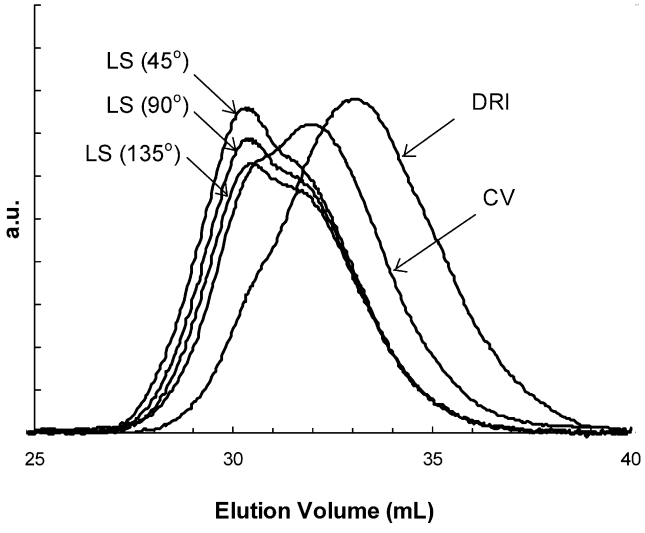

Fig. 1. SEC traces from three-angle laser light scattering, DRI and viscosity detectors for CGC1 with LCBF of 0.98 and LCBD of 2.88 br/10,000 C.

$$M = \left(\frac{K^*C}{R_\theta}\right)^{-1}_{\theta\to 0} \tag{4}$$

$$\langle r_g^2\rangle = \frac{3m_0\lambda_0^2 M}{16\pi^2} \tag{5}$$

where

$$m_0 = \mathrm{d}[K^*C/R_\theta]/\mathrm{d}[\sin^2(\theta/2)]_{\theta\to 0}.$$

The number- and mass-average mean square radii of gyration, as well as the mass-average intrinsic viscosity, were calculated using the following equations:

$$\langle r_g^2\rangle_n = \frac{\sum\left(\frac{C_i}{M_i}\langle r_g^2\rangle_i\right)}{\sum\left(\frac{C_i}{M_i}\right)} \tag{6}$$

$$\langle r_g^2\rangle_w = \frac{\sum(C_i\langle r_g^2\rangle_i)}{\sum C_i} \tag{7}$$

$$[\eta]_w = \frac{\sum(C_i[\eta]_i)}{\sum C_i} \tag{8}$$

3. Results and discussion

3.1. GPC analysis of linear PE samples and accuracy of the method

The mass-average molecular masses of the seven polystyrene (PS) standards with molecular mass in the range (from 3 to 109)×10^6 g/mol were determined by the LS and DRI detectors. Compared to the reported values, an average standard deviation of ±1.9% and a maximum of ± 3.4% were observed (unless otherwise noted, the ± represents uncertainties of the measured values and refers to one standard deviation of the observed value). Two different runs for the NBS 1475a linear PE were also conducted and the molecular mass data reported in Table 1. The M_w from the LS/DRI detectors was 5.22×10^4 g/mol. The uncertainty of this measurement was less than 1% relative to the reported value of 5.20×10^4 g/mol.

Using the universal calibration curve of PS standard samples, $([\eta]M)_{PE} = ([\eta]M)_{PS} = f(\text{retention volume})$, for NBS 1475a (the average values of the two repeats) the CV/DRI detectors produced M_n, M_w and M_z of 1.98×10^4, 5.23×10^4 and 1.34×10^5, respectively, which were comparable with the reported data of 1.83×10^4, 5.31×10^4 and 1.38×10^5. The average molecular masses of Zr1-4 samples calculated from the CV/DRI data are reported in Table 1. The mean relative deviation by M_w was 10.7%.

The use of the Mark-Houwink parameters of PE samples measured by LS/CV detectors helps minimizing experimental errors. The reliable signals for all five PE samples

Table 1
Average molecular masses, intrinsic viscosity and root mean-square radii for linear polyethylene samples

Sample	CV				LS					
	M_n (g/mol)	M_w (g/mol)	M_z (g/mol)	$[\eta]$ (g/dl)	M_n (g/mol)	M_w (g/mol)	M_z (g/mol)	$\langle r_g^2\rangle_n^{1/2}$ (nm)	$\langle r_g^2\rangle_w^{1/2}$ (nm)	$\langle r_g^2\rangle_z^{1/2}$ (nm)
NBS 1475a[a]	1.831×10^4	5.307×10^4	1.380×10^5	–	–	5.200×10^4	–	–	–	–
NBS 1475a[b]	1.967×10^4	5.253×10^4	1.384×10^5	1.025	1.934×10^4	5.249×10^4	1.551×10^5	10.4	15.3	26.2
	1.986×10^4	5.209×10^4	1.296×10^5	1.030	1.954×10^4	5.196×10^4	1.453×10^5	10.0	15.0	24.8
Zr1	1.104×10^4	2.776×10^4	4.666×10^4	0.623	1.303×10^4	2.408×10^4	3.618×10^4	9.4	11.3	12.7
Zr1[c]	1.039×10^4	2.392×10^4	3.853×10^4							
Zr2	2.790×10^4	5.842×10^4	9.790×10^4	1.098	2.834×10^4	5.370×10^4	8.216×10^4	9.9	14.5	18.1
Zr2[c]	2.726×10^4	5.264×10^4	8.389×10^4							
Zr3	2.847×10^4	6.077×10^4	1.008×10^5	1.110	3.022×10^4	5.533×10^4	8.284×10^4	11.1	14.9	18.3
Zr3[c]	2.703×10^4	5.387×10^4	8.591×10^4							
Zr4	2.004×10^4	4.286×10^4	7.034×10^4	0.885	2.181×10^4	3.932×10^4	5.967×10^4	8.6	11.9	14.9
Zr4[c]	1.940×10^4	3.888×10^4	6.163×10^4							

[a] Reported values.
[b] Values from our measurements.
[c] Calculation using K and α values in Eq. (10).

(NBS 1475a and Zr1-4) were combined for the analysis and were found to overlap well. The Mark-Houwink expression was found to be:

$$[\eta] = 5.23\times10^{-4}\,M^{0.710} \text{ for } M \text{ in the range } (3\times10^4 \le M \le 5\times10^5) \quad (9)$$

The parameter values are in agreement with the earlier reports [11,17]. These constants were subsequently used to calculate the molecular masses from the CV/DRI data for the samples Zr1-4 and the results were also listed in Table 1. And while the values were similar to those from the LS/DRI detectors, the mean relative deviation was reduced to 1.6%.

In a dilute polymer solution, the correlation between $\langle r_g^2\rangle^{1/2}$ and M can be expressed as $\langle r_g^2\rangle^{1/2} \propto M^{\beta}$, [16] where β is a constant in the range of (0.33–1.0) and is determined by the geometry of gyration. It is 0.5 for an unperturbed coil of a linear chain in a θ-solvent and 0.588 in a good solvent [16].

The following relationship between $\langle r_g^2\rangle^{1/2}$ and M that held for all linear PEs was found:

$$\langle r_g^2\rangle^{1/2} = 2.86\times10^{-2}\,M^{0.568} \text{ for } M \text{ in the range } (2.5\times10^4 \le M \le 9\times10^5) \quad (10)$$

Note that we obtain the β value that is in agreement with the earlier studies: $\beta \approx (0.575–0.590)$ [11,12] for the linear PE in TCB at 135 °C. For the non-free draining case [16], the following Fox–Flory relationship applies,

$$[\eta] = \Phi\left(\frac{(\langle r_g^2\rangle^{1/2})^3}{M}\right) \quad (11)$$

where Φ is a proportionality factor. Substituting Eqs. (9) and (10) into Eq. (11) yields a relationship: $\alpha = 3\beta - 1$. In Eq. (10), $\beta = 0.568$, therefore, $3\beta - 1 = 0.704$, which is close to $\alpha = 0.710$.

Table 2
Intrinsic viscosity, average molecular masses, and root mean-square radii for long-chain branched polyethylenes

Sample	LCBF	$[\eta]$ (g/dl)	LS					
			M_n (g/mol)	M_w (g/mol)	M_z (g/mol)	$\langle r_g^2\rangle_n^{1/2}$ (nm)	$\langle r_g^2\rangle_w^{1/2}$ (nm)	$\langle r_g^2\rangle_z^{1/2}$ (nm)
CGC1	0.98	1.514	4.868×10^4	1.413×10^5	4.490×10^5	17.0	23.3	38.6
CGC2	0.16	1.601	5.417×10^4	1.023×10^5	1.763×10^5	16.7	20.7	26.2
CGC3	0.14	1.576	5.451×10^4	1.005×10^5	1.690×10^5	15.8	20.2	25.9
CGC4	0.12	1.589	5.329×10^4	9.888×10^4	1.654×10^5	15.1	19.9	25.6
CGC5	0.11	1.424	4.311×10^4	8.313×10^4	1.371×10^5	14.2	18.4	23.2
CGC6	0.07	1.502	4.725×10^4	8.611×10^4	1.354×10^5	15.8	19.3	23.8
CGC7	0.06	1.427	4.523×10^4	7.844×10^4	1.231×10^5	16.2	18.8	22.8
CGC8	0.06	1.577	5.156×10^4	8.914×10^4	1.507×10^5	15.5	19.3	23.8
CGC9	0.07	1.822	6.416×10^4	1.143×10^5	1.787×10^5	17.1	22.1	27.8
CGC10	N/A	1.503	4.064×10^4	1.315×10^5	4.502×10^5	14.8	21.9	38.5
CGC11	N/A	1.594	5.169×10^4	9.762×10^4	1.635×10^5	16.2	20.2	25.4
CGC12	N/A	1.498	4.800×10^4	9.149×10^4	1.450×10^5	14.9	19.5	24.5
B1	0.09	1.698	5.669×10^4	1.066×10^5	1.676×10^5	15.2	20.6	26.0
B2	0.08	2.164	8.044×10^4	1.496×10^5	2.502×10^5	19.1	25.6	32.6

3.2. Contraction factors of branched PE samples

As determined by the ^{13}C NMR [1,10], 14 LCB PE samples had the LCBD of (0.20–2.88) carbons per 10,000 C, and the LCBF of (0.06–0.98) branches per polymer chain. Table 2 summarizes the LCBF, the average intrinsic viscosity and molecular masses, as well as the root mean-square radii of gyration.

The $\langle r_g^2\rangle^{1/2}$ and $[\eta]$ versus the molecular mass for CGC1, CGC2 and CGC9 (with LCBF of 0.98, 0.16 and 0.07, respectively) are presented in Fig. 2. Note that the molecular mass of GPC elution fraction, m.w., in the x-axis of figures should not be confused with the mass-average molecular mass of sample in the text, M_w. The data for the linear PE (Eqs. (9) and (10)) are also shown in this figure. The branched samples (CGC1 and CGC2) had lower $\langle r_g^2\rangle^{1/2}$ and $[\eta]$ values than the linear ones. However, the CGC9 sample (with LCBF of 0.07) was almost indistinguishable from the linear PE, pointing at the sensitivity limits of both of the detectors.

The information about branching can be represented by the contraction factors g and g', calculation of which is based on how $\langle r_g^2\rangle$ and $[\eta]$ scale with M for linear PEs. The g and g' values for CGC1, CGC2 and CGC9 were calculated by dividing the $\langle r_g^2\rangle$ and $[\eta]$ data of branched samples by those of linear ones of the same total molecular mass (Fig. 3). Clearly, samples with higher LCBF have lower g and g' values.

The relationship between g and g' can be expressed as follows,

$$g' = g^{\varepsilon} \tag{12}$$

where ε is an exponential factor, the magnitude of which depends on both branch type and experimental conditions. It is 0.5 for a non-free drain star polymers and 1.5 for a comb

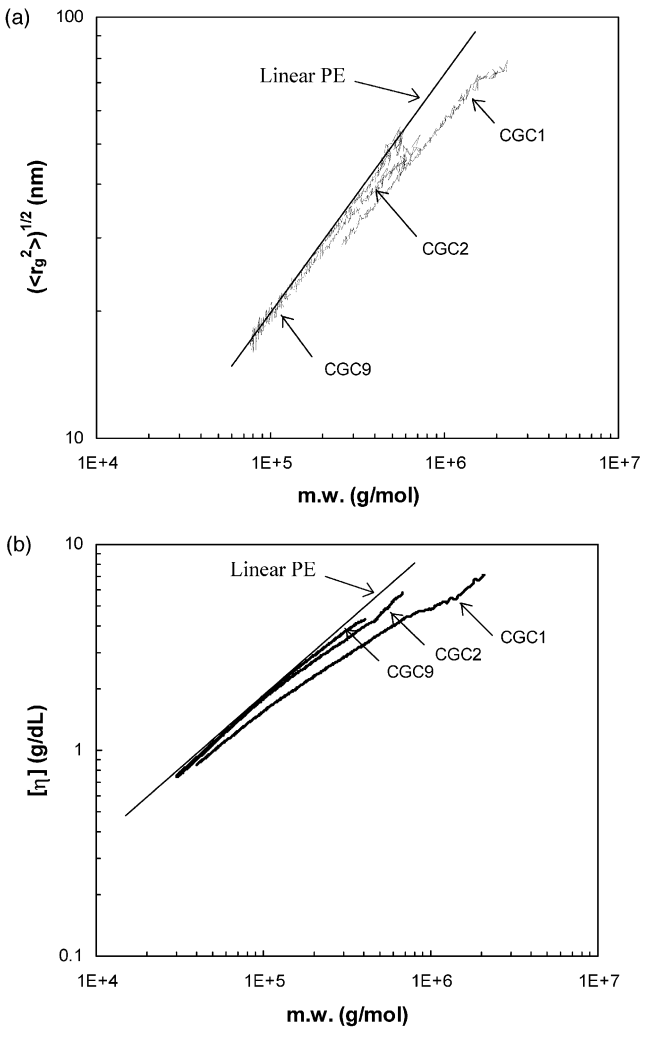

Fig. 2. Root mean-square radius of gyration $(\langle r_g^2\rangle)^{1/2}$ (a) and intrinsic viscosity ($[\eta]$) (b) as a function the molecular mass of GPC elution fraction for linear and LCB polyethylenes with LCBF of 0.98 (CGC1), 0.16 (CGC2) and 0.07 (CGC9).

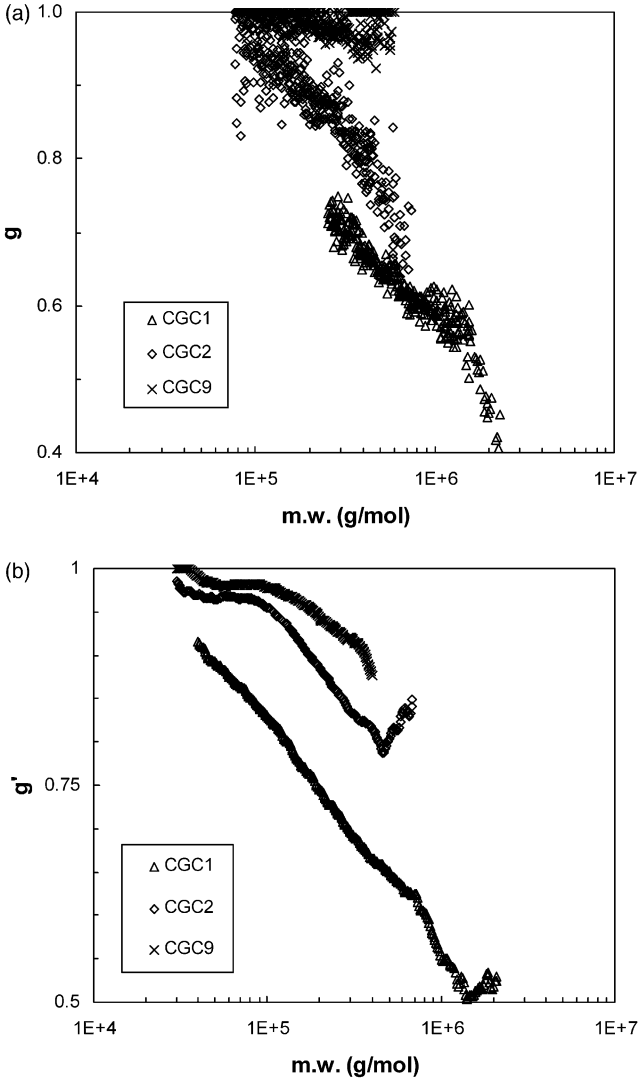

Fig. 3. Contraction factors g (a) and g' (b) as a function of the molecular mass of GPC elution fraction for LCB polyethylene samples with LCBF of 0.98 (CGC1), 0.16 (CGC2) and 0.07 (CGC9).

polymer with side chains shorter than the backbone [12,18]. The reported values were (from 0.5 to 2.0) for low density polyethylenes (LDPE) [12,19–21]. In calculation of ε, only g and g' values smaller than 0.95 were considered. Most of ε data for LCB PEs in the molecular mass range of (10^5 to 10^6) g/mol were between 1.8 and 0.2. The ε data for CGC(1-5), CGC9, CGC11 and B2 are plotted against M in Fig. 4. As it can be seen, ε has a strong molecular mass dependence. The higher molecular mass chains have lower ε values for all the samples, except for the CGC1 that showed a linear dependence with M for $M<10^5$ g/mol. Using the following expressions, the number- and mass-average g and g' values were calculated and presented in Table 3,

$$g_n = \frac{\sum_i g_i \frac{C_i}{M_i}}{\sum_i \frac{C_i}{M_i}} \quad g_w = \frac{\sum_i g_i C_i}{\sum_i C_i} \tag{13}$$

The ε_n and ε_w values were in the (0.62–2.51) and (0.94–1.63) ranges, respectively.

The factor Φ in the Fox-Flory relationship (Eq. (11)) is greatly influenced by the inter-particle hydrodynamic interaction [16] For linear PE samples (NBS 1475a and Zr1-4), the Φ values were $(2.33\pm0.10)\times10^{25}$, and for CGC(1-5), CGC9, CGC11 and B2 they are estimated in Fig. 5. For M from $(2.31\times10^4$ to 2.86×10^6) g/mol, Φ was in the range of $(1.43–3.10)\times10^{25}$. For higher molecular mass fractions these values were slightly higher than that of linear polymers, showing the effect of branches on the inter-particle hydrodynamic interaction. Since Φ increases with M, it suggests that the hydrodynamic volume of the branched polymers increased more strongly with M than with the radius of gyration.

3.3. Molecular mass dependence of branching density

Although both g and g' can be used to interpret information about branching, the application of g' requires the understanding of the hydrodynamic interactions among the chain segments. The former is more convenient for analyzing the branch distribution because it does not require an additional approximation [16]. The ^{13}C NMR measurement indicated that there was only a T-type of branching in the CGC PEs [1,5,15]. The kinetic study also elucidated the random long-chain branching mechanism [1,10,28]. We thus applied the following Zimm–Stockmayer equation [23] to calculate the LCBF,

$$g = \left[\left(1+\frac{\mathrm{LCBF}}{7}\right)^{1/2} + \frac{4\times\mathrm{LCBF}}{9\pi}\right]^{-1/2} \tag{14}$$

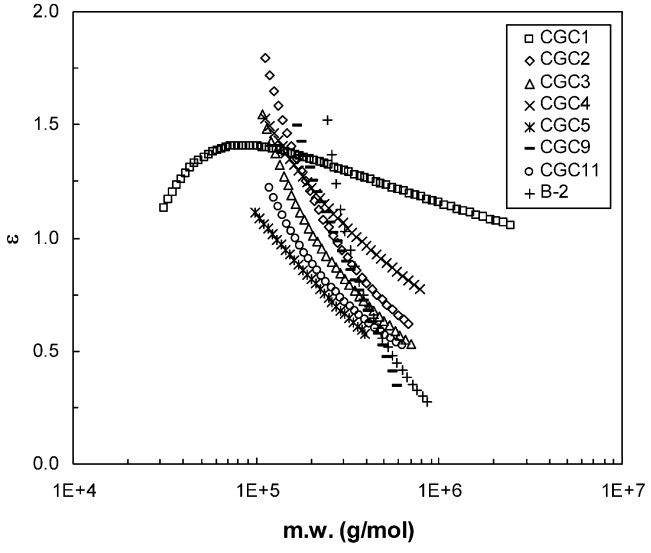

Fig. 4. Dependence of the contraction exponent ε ($g'=g^{\varepsilon}$) on the molecular mass for LCB PEs.

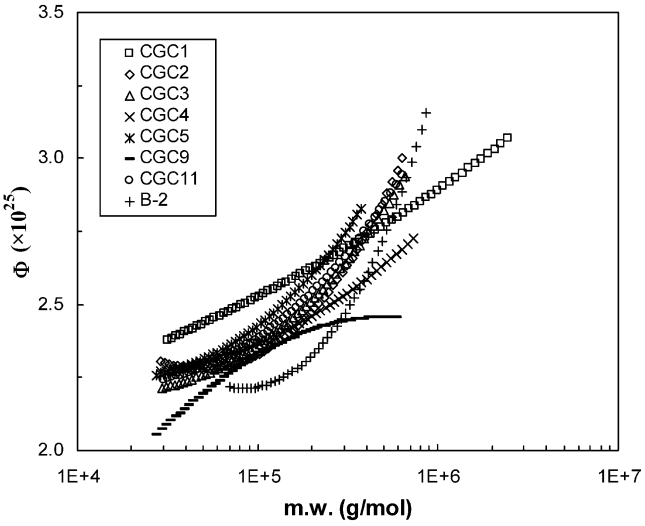

Fig. 5. Dependence of the Fox–Flory factor (Φ) on the molecular mass for LCB PEs.

Fig. 6a shows the molecular mass dependence of LCBF for CGC1, CGC2, CGC5 and CGC9 (with LCBF of 0.98, 0.16, 0.11 and 0.07, respectively). Note that the highest molecular mass fractions had more than one branch per polymer molecule, and LCBF increased with M. The dependence of long chain branching on M shown in the figure deserves a particular attention. This particularly concerns the longest chains that apparently have a complex branch structure. In fact, they contain up to tens of branches per polymer molecule. The question is whether the number of branch structures increases linearly with the molecular mass, that is whether doubling the molecular mass would double the number of branches. Fig. 6(b) shows the dependence of LCBD on M. Note that for highly branched CGC1 sample, the LCBD decreased with M in the measured range. However, for sparsely branched samples (CGC2, CGC5, and CGC9) the branch density appears to be the highest in the range of medium molecular masses.

In the solution polymerization of ethylene LCB occurs through a macromonomer mechanism. A chain generated by the chain transfer to ethylene or beta-hydride elimination bears a terminal vinyl group that can be incorporated into a

Table 3
Comparison of the long-chain branch densities and frequencies determined by the ^{13}C NMR and light scattering for LCB polyethylenes

Sample	^{13}C NMR		LS/CV							
	LCBD /C/ 10^4 C	LCBF	LCBD /C/ 10^4 C	LCBF	g_n	g_w	g'_n	g'_w	ε_n	ε_w
CGC1	2.88	0.98	3.22	0.98	0.916	0.847	0.947	0.849	0.62	0.99
CGC2	0.44	0.16	0.46	0.17	0.984	0.958	0.975	0.940	1.57	1.44
CGC3	0.40	0.14	0.39	0.15	0.986	0.962	0.981	0.951	1.36	1.30
CGC4	0.35	0.12	0.36	0.13	0.988	0.964	0.984	0.953	1.33	1.31
CGC5	0.35	0.11	0.38	0.13	0.988	0.966	0.991	0.968	0.75	0.94
CGC6	0.22	0.07	0.26	0.09	0.991	0.975	0.991	0.974	1.00	1.04
CGC7	0.21	0.06	0.18	0.06	0.994	0.989	0.994	0.983	1.00	1.55
CGC8	0.20	0.06	0.13	0.05	0.995	0.992	0.995	0.987	1.00	1.63
CGC9	0.20	0.07	0.11	0.05	0.996	0.987	0.990	0.980	2.51	1.54
CGC10	N/A	N/A	0.90	0.23	0.983	0.906	0.966	0.876	2.01	1.34
CGC11	N/A	N/A	0.36	0.13	0.988	0.966	0.984	0.962	1.33	1.12
CGC12	N/A	N/A	0.34	0.12	0.989	0.966	0.980	0.950	1.83	1.48
B1	0.23	0.09	0.28	0.10	0.990	0.972	0.985	0.961	1.50	1.40
B2	0.22	0.08	0.10	0.05	0.995	0.979	0.993	0.976	1.40	1.14

growing molecule by insertion from a branch point. The probability of the macromonomer insertion appears to be molecular mass dependent, which is evident from this triple detector array in the GPC measurement. It is more difficult for a high molecular mass macromonomer to be inserted than for its lower molecular mass counterpart. This difficulty may be caused by the diffusion limitations of the high molecular mass chain. These limitations reduce the effective reactivity of the terminal vinyl group and result in lower LCBD at higher molecular masses. Therefore, the high molecular mass chains may have a 'branch-on-branch' topology. In contrast to that the architecture in the range of medium molecular masses is 'comb-like', as indicated by the low ε values in Fig. 4.

On the other hand, PE chains of the lowest molecular masses are linear. Fig. 6(b) shows that the chains with molecular mass lower than a certain value contained no branch structures (e.g. zero LCBD). This critical value of molecular mass decreased with the increase of the average branching density of the sample: CGC9, CGC5 and GGC2 had the critical molecular mass of (8.3, 4.9 and 2.1)$\times 10^4$ g/mol, respectively, corresponding to an average LCBD of 0.44, 0.35 and 0.20 branches per 10,000 carbons. The sample CGC1 with an average LCBD of 2.88 br/10,000 C was an exception that did not show this low molecular mass part probably because the data were out of the GPC range.

In order to compare our findings to the ^{13}C NMR measurements, the average LCBF and LCBD were calculated by

$$\mathrm{LCBF} = \frac{\sum_i \mathrm{LCBF}_i \frac{C_i}{M_i}}{\sum_i \frac{C_i}{M_i}} \tag{15}$$

$$\mathrm{LCBD} = \frac{140,000 \times \sum_i \mathrm{LCBF}_i \frac{C_i}{M_i}}{\sum_i C_i} \tag{16}$$

This information is summarized in Table 3. The estimates from the LS detector were in good agreement with the ^{13}C NMR measurements for PEs with LCBF greater than 0.08 or LCBD greater than 0.22. Due to sensitivity limitations of the LS technique the errors for samples having LCBF less than 0.08 were quite significant.

3.4. Rheology and processing of LCB PE

It is well established that molecular architecture, particularly branching, is critical to polymer flow behavior and its processing [29–31]. The molecular topology controls the relaxation of polymer chains in the limit of linear viscoelasticity and leads to some spectacular consequences in non-linear flows [32,33]. One of the most widely used branched polymers that is known to exhibit the non-linear *strain-hardening* as well as strong shear thinning behavior and which is particularly relevant to the manufacture of commodity plastics, is low density polyethylene (LDPE). This is a highly branched polymer with a poorly defined topology: it has a wide molecular mass distribution and an irregular branching pattern. The lack of information regarding the molecular mass or molecular mass distribution for this material presents additional difficulties in devising the correlative structure-property relationships. However, the processing characteristics of LDPE have long been recognized to be superior to conventional high density polyethylene (HDPE) and linear low density polyethylene (LLDPE) in that the flow instabilities, such as sharkskin, were reported to be delayed to much higher shear rates, or even eliminated completely [34,35]. Similar qualitative observations were made in polyethylenes in which LCB was *sparse* i.e. each polymer chain contained fewer (on the average) than 1 branch point [36,37]. While there is presently no unified information about the origin of the improved processability of both highly and sparsely branched PEs, it is perceived that the elongational strength

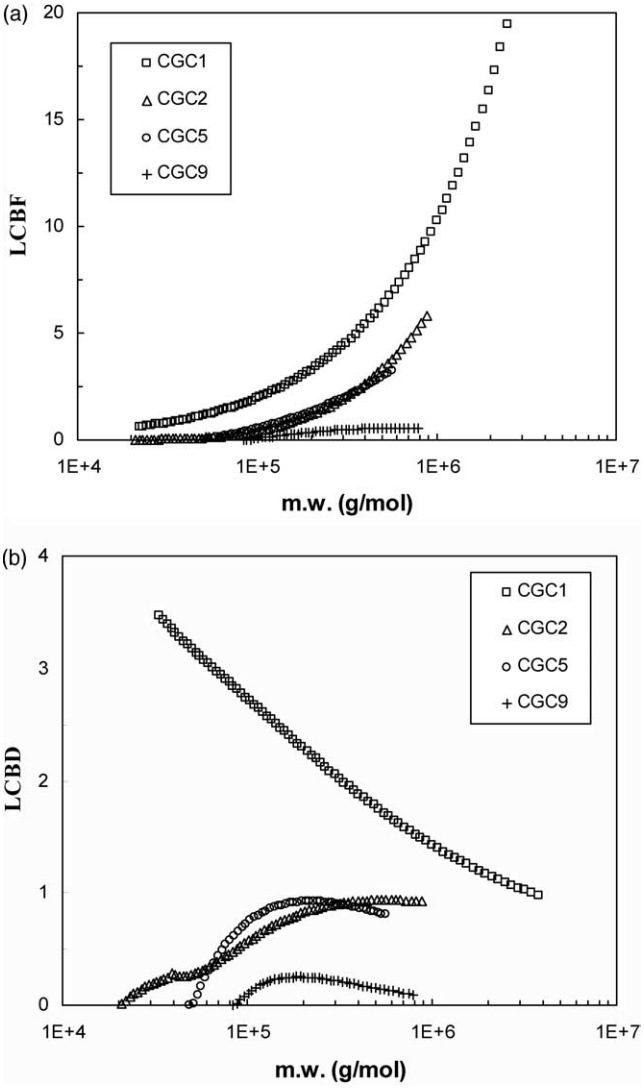

Fig. 6. Molecular mass dependence of the LCBF (a) and LCBD (b) for several LCB PEs.

(or strain-hardening behavior) may be a major contributor to this effect [37].

In our work, the information about the distribution of long-chain branches with polymer molecular mass (Fig. 6(a) and (b)) offers an opportunity to study the impact of molecular topology on the polymer flow and processing behavior. A set of relevant experiments has been performed at NIST's Polymers Division. First, we characterize the basic melt rheology properties of LCB PEs in steady and oscillatory shear flows.

Fig. 7 shows the frequency dependence of the storage component of the shear stress (G') as a function of LCBD for two LCB PEs. A linear low-density polyethylene (LLDPE) produced by Exxon-Mobil [38] with a mass average molecular mass of 80,000 g/mol and a melt flow index of 1.0 was also tested for comparison. This polymer is also known to contain short-chain branches (butene). The measurements were done at a temperature of 180 °C and

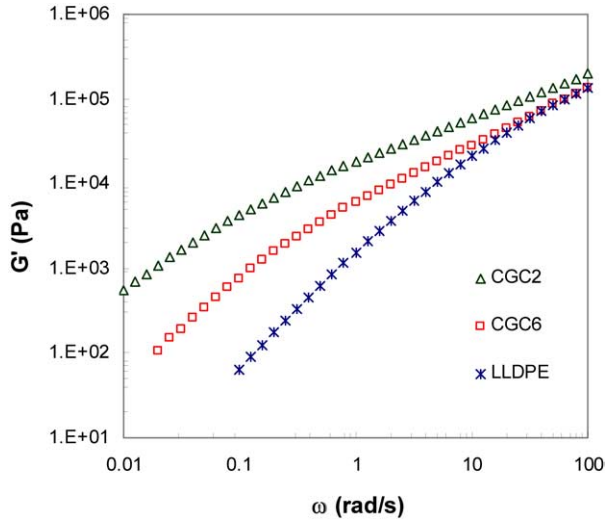

Fig. 7. Elasticity of LCB PEs. $T = 180$ °C.

within the range of linear viscoelasticity (25-mm parallel plates of the ARES rheometer set at a gap of about 1 mm were used). An anticipated trend of the increased elasticity of LCB PEs is shown in Fig. 7 and a similar enhancement is found in the frequency dependence of the complex viscosity (Fig. 8). Since the molecular masses of CGC2, CGC6 and LLDPE are known and the molecular mass distributions of the LCB PEs are fairly low and comparable (Table 2), and since the presence of short-chain branches in LLDPE has a negligible effect on polymer viscoelasticity [39], such responses suggest that the relaxation modes for these polymers have additional contributions with origins in the long-chain branching density [39]. Finally, our capillary viscometry, done using a Goettfert Rheo-Tester 2000 rheometer and a tungsten carbide cylindrical die (with a length-to-diameter ration, L/D = 30 and a die entrance angle of 180°), overlap well with the corresponding oscillatory

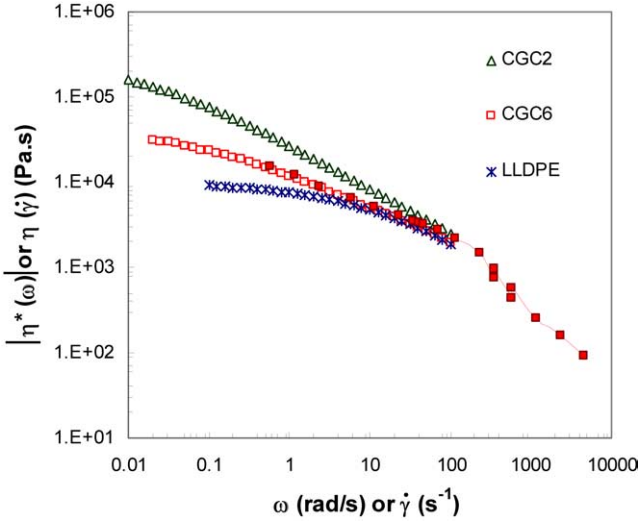

Fig. 8. Viscosity of LCB PEs. Note that the filled symbols fitted with the solid lines represent the capillary rheometry measurements. $T = 180$ °C.

shear data (Fig. 8). The overlap confirms the applicability of the empirical Cox-Merz rule [40]. This finding is in accord with the earlier works on sparsely branched PEs [37,39].

In spite of the similarities in the basic rheological properties of the LCB PEs in our work with the previously reported studies, we acknowledge a striking observation noted in the processing of these materials. Particularly, when extruded through a cylindrical die, all of the LCB PEs exhibited characteristic to LLDPE and HDPE flow instabilities (Fig. 9). Moreover, the severity of the instabilities increased for LCB PEs with higher branching frequencies. Table 4 lists the critical apparent shear rate and wall shear stress at which the sharkskin melt fracture, stick-slip and gross melt fracture first onset for these polymers. This result is in contrast to earlier works in which polyethylenes with a relatively small but comparable contents of the long-chain branches [36,37] were processed with the improved characteristics. Additionally, we have tested the rheology and processability of the Dow Chemical Affinity PL 1840, a commercial grade polyethylene that contains $0.57/10^4$ C long-chain branches as well as short-chain branches (octene). It is a moderately disperse polymer ($M_w/M_n=$ 2.43) with a comparable molecular mass ($M_w=87.4$ kg/mol) to that of the model LCB PEs in our work. Similar to commercial grade LDPE and LCB PE [34–37], this polymer also showed improved processing characteristics (compared to the PEs in the present study): the sharkskin onset (at 180 °C) was at the apparent shear rate of approximately 120 s^{-1} (and the wall shear stress of 185 kPa), which is substantially higher than the critical parameters reported in Table 4. Concomitantly, this material is also known to exhibit the strain-hardening behavior in extensional deformations [41].

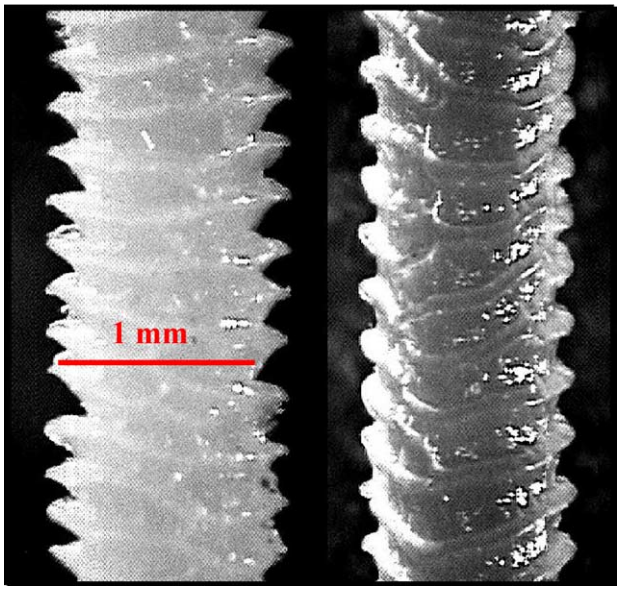

Fig. 9. Sharkskin melt fracture of 0.44 LCB PE (left) and LLDPE (right) extrudates. Both of the samples were extruded at an apparent shear rate of 230 s^{-1} and a temperature of 180 °C.

Presently, the origin of the significant discrepancy in the processing behavior between our model LCB PEs and the commercial grade branched PEs is not clear. It may be attributed to a unique branch type that resulted from using our CGC catalyst. The analysis is further complicated by the conflicting reports in the literature. For example, from the study by Fernández and co-workers [42] as well as Hatzikiriakos et al. [43] it can be implied that for a set of sparsely branched PEs the melt fracture occurs approximately at the same level of the wall shear stress. Also, from the former study [42], it follows that the materials with the higher content of LCB exhibit the melt fracture at lower shear rates. While similar observations regarding the comparable wall shear stresses for the onset of instability can be made in the work by Kim et al. [36], the authors report that the critical shear rate for the onset of melt fracture for PEs with the higher concentration of long-chain branches increases rather than decreases. Yet, no information on the molecular mass of their LCB PEs was provided. In contrast to these works, Venet and Vergnes [37] showed that the onset of melt fracture for LCB PEs in their study apparently occurs at a different magnitude of the wall shear stress. However, they used γ irradiation to obtain long chain branching.

It is known that the branch architectures emanating from the metallocene-catalyzed synthesis can have a wide range of molecular topologies [44]. It is also known that the topological class of the branched melt (T- or H-type of architectures), the molecular mass between the branch points and the content of interior chains [33] couple the LCBF and branch length to rheology and processing behavior in a different way [45]. Unfortunately, the lack of information on either the type, frequency or the distribution of long-chain branches in the abovementioned studies makes it difficult to develop predictive structure-property relationships as well as draw any quantitative comparisons with the present work.

4. Conclusion

A size exclusion chromatograph (SEC) coupled with three on-line detectors: the three-angle laser light scattering (LS), differential refractive index (DRI) and the viscometer (CV) was used to characterize fourteen LCB and five linear PE samples prepared by the solution polymerization of ethylene. The PE samples had low levels of long-chain branching with LCBF of (0.06–0.98). The elucidation of LCB was based on the $\langle r_g^2\rangle^{1/2}$ and $[\eta]$ for the branched samples in reference to linear ones. For the linear PEs, a correlation of $\langle r_g^2\rangle^{1/2} \propto M_w^{\beta}$ with β of 0.568 was established and the Mark-Houwink constants K and α were 5.23×10^{-4} and 0.710, respectively. The contraction factors (g and g') of the branched samples, as well as the exponential factor (ε), strongly depended on the branch level and branch type. The ε values varied from 1.8 to 0.2 in the molecular mass range

Table 4
Effect of the molecular architecture on the critical shear rate and wall shear stress at the onset of the flow instability

LCBD/C/10^4 C	Sharkskin		Stick/slip	GMF (est.)
	$\dot{\gamma}(s^{-1})$	σ (kPa)	$\dot{\gamma}$ (s^{-1})	$\dot{\gamma}$ (s^{-1})
0 (LLDPE)	46	138	460	
0.22 (CGC6)	43	140	345	
0.35 (CGC5)	35	148	201	>800
0.35 (CGC4)	29	138	190	
0.40 (CGC3)	23	116	173	
0.44 (CGC2)	17	107	144	

of (10^5 to 10^6) g/mol with the lower molecular mass chains having more comb-like structure. The factor Φ in the Fox-Flory relationship for the LCB PEs varied from (1.43–3.10)$\times 10^{25}$, suggesting that the LCB chains have significant inter-particle hydrodynamic interactions.

The Zimm-Stockmayer equation for randomly distributed T-type branching was used to estimate LCBF and LCBD of each elution fraction for the branched samples. A good agreement between the triple detector array GPC data and ^{13}C NMR measurements was achieved for the average LCBF and LCBD values. The LCB in solution polymerization of ethylene was found to be molecular mass dependent. The higher molecular mass chains contained more branches in terms of an absolute number. However, in terms of the branching density, the maximum was in the range of medium molecular masses. Very low molecular mass chains were essentially linear. The branch structure started to appear only when the molecular mass reached a critical value. The branch density increased with the increase of the molecular mass only in the range of low molecular masses. In the high molecular mass range, the density decreased probably because of the diffusion limitations of high molecular mass PE macromonomers involved in the branching mechanism.

From the rheological measurements it was found that the long chain branching significantly increased the low-frequency storage modulus and enhanced the shear-thinning behavior. However, no improvement in the materials melt flow stability was observed. The critical apparent shear rate and the wall shear stress at which the sharkskin and stick-slip melt fracture first onset for these polymers both decreased with LCBD, perhaps suggesting that the H-type of branching did not result from using our unique CGC catalyst. Experiments probing the material properties in the extensional flows will likely shed more light on this unusual flow instability behavior.

Acknowledgements

We thank the National Institute of Standards and Technology (NIST) for supporting this research and the Canada Foundation of Innovation (CFI) for supporting the facilities.

References

[1] Wang W-J, Yan D, Zhu S, Hamielec AE. Macromolecules 1998;31:8677.
[2] Yan D, Wang W-J, Zhu S. Polymer 1999;40:1737.
[3] Malmberg A, Kokko E, Lehmus P, Löfgren B, Seppälä JV. Macromolecules 1998;31:8448.
[4] Shroff RN, Mavridis H. Macromolecules 1999;32:8454.
[5] Wang WJ, Zhu S, Park S. Macromolecules 2000;33:5770.
[6] Kolodka E, Wang W-J, Charpentier PA, Zhu S, Hamielec AE. Polymer 2000;41:3985.
[7] Vega JF, Muñoz-Escalona A, Santamaría A, Muñoz ME, Lafuente P. Macromolecules 1996;29:960.
[8] Dayal U. J Appl Polym Sci 1994;53:1557.
[9] Pang S, Rudin A. J Appl Polym Sci 1992;46:763.
[10] Wang W-J, Yan D, Zhu S, Hamielec AE. Polym React Engng 1999;7:327.
[11] Hadjichristidis N, Xenidou M, Iatrou H, Pitsikalis M, Poulos Y, Avgeropoulos A, Sioula S, Paraskeva S, Velis G, Mendelson RA, Garcia-Franco CA, Sun T, Ruff CJ. Macromolecules 2000;33:2424.
[12] Tackx P, Tacx JC. Polymer 1998;39:3109.
[13] Chum PS, Kao CI, Knight GW. Plast Engng 1995;51:21.
[14] Randall JC. J Macromol Sci, Rev Macromol Chem Phys 1989;C29:201.
[15] Wang W-J, Zhu S. Macromolecules 2000;33:1157.
[16] Burchard W. Adv Polym Sci 1999;143:113.
[17] Scholte TG, Meijerink NLJ, Schoffeleers HM, Brands A. J Appl Polym Sci 1984;29:3763.
[18] Scholte TG. In: Dawkins JV, editor. Developments in polymer characterization, vol. 4. Essex: Applied Science; 1984. Chapter 1.
[19] Kuhn R, Kromer H, Rosmanith G. Angew Makromol Chem 1974;40:361.
[20] Kuhn R, Kromer H. Colloid Polym Sci 1982;260:1083.
[21] Scholte TG, Meijerink NLJ. Br Polym J 1974;133:9.
[22] Cotts PM, Cuan Z, McCord E, McLain S. Macromolecules 2000;33:6945.
[23] Zimm BH, Stockmayer WH. Chem Phys 1949;17:1301.
[24] Stockmayer WH, Fixman M. Ann NY Acad Sci 1953;57:334.
[25] Charpentier PA, Zhu S, Hamielec AE, Brook M. Ind Engng Chem Res 1997;36:5074.
[26] MacRury TB, McConnell ML. J Appl Polym Sci 1979;24:651.
[27] Zimm BH. J Chem Phys 1948;16:1093.
[28] Wang W-J, Kolodka EB, Zhu S, Hamielec AE. J Polym Sci, Polym Chem 1999;37:2949.
[29] Munstedt H, Laun HM. Rheol Acta 1999;20:211.
[30] Khan SA, Larson RG. J Rheol 1987;31:207.
[31] Laun HM, Schuch H. J Rheol 1989;33:119.
[32] Bick DK, Mcleish TCB. Phys Rev Lett 1996;76:2587.
[33] Kasehagen LJ, Macosko CW. J Rheol 1998;42:1303.
[34] Bergem N. VIIth International Congress of Rheology 1976 p. 50–54.
[35] Mackley MR, Rutgers RPG, Gilbert DG. J Non-Newtonian Fluid Mech 1998;76:281.
[36] Kim YS, Chung CI, Lai SY, Hyun KS. J Appl Polym Sci 1996;59:125.

[37] Venet C, Vergnes B. J Rheol 1997;41:873.
[38] Certain equipment, instruments or materials are identified in this paper in order to adequately specify the experimental details. Such identification does not imply recommendation by the National Institute of Standards and Technology nor does it imply the materials are necessarily the best available for the purpose.
[39] Wood-Adams PM, Dealy JM, deGroot AW, Redwine OD. Macromolecules 2000;33:7489.
[40] Ferry JD. Viscoelastic properties of polymers. New York: Wiley; 1980.
[41] Doerpinghaus PJ, Baird DG. J Rheol 2003;47:717.
[42] Fernandez M, Vega JF, Santamaria A, Munoz-Escalona A, Lafuente P. Macromol Rapid Commun 2000;21:973.
[43] Hatzikiriakos SG, Kazatchkov IB, Vlassopoulos D. J Rheol 1997;41:1299.
[44] Benedikt GM, Goodall BL. Metallocene catalyzed polymers: materials, properties, processing and markets. New York: Plastics Design Library; 1998.
[45] Crosby BJ, Mangnus M, de Groot W, Daniels R, Mcleish TCB. J Rheol 2002;46:401.